



## Second harmonic generation from metamaterials strongly coupled to intersubband transitions in quantum wells

Salvatore Campione, Alexander Benz, Michael B. Sinclair, Filippo Capolino, and Igal Brener

Citation: [Applied Physics Letters](#) **104**, 131104 (2014); doi: 10.1063/1.4870072

View online: <http://dx.doi.org/10.1063/1.4870072>

View Table of Contents: <http://scitation.aip.org/content/aip/journal/apl/104/13?ver=pdfcov>

Published by the [AIP Publishing](#)

---

### Articles you may be interested in

[Orthogonally twisted planar concentric split ring resonators towards strong near field coupled terahertz metamaterials](#)

*Appl. Phys. Lett.* **104**, 101105 (2014); 10.1063/1.4868122

[Tunable metamaterials based on voltage controlled strong coupling](#)

*Appl. Phys. Lett.* **103**, 263116 (2013); 10.1063/1.4859636

[Intersubband resonant enhancement of secondharmonic generation in GaN/AlN quantum wells](#)

*AIP Conf. Proc.* **893**, 483 (2007); 10.1063/1.2729976

[Intersubband resonant enhancement of second-harmonic generation in Ga N Al N quantum wells](#)

*Appl. Phys. Lett.* **89**, 151101 (2006); 10.1063/1.2358118

[Quasiphase matched surface emitting second harmonic generation in periodically reversed asymmetric GaAs/AlGaAs quantum well waveguide](#)

*Appl. Phys. Lett.* **70**, 2655 (1997); 10.1063/1.118987

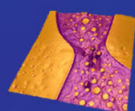
---

## Asylum Research Atomic Force Microscopes

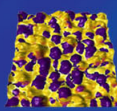
*Unmatched Performance, Versatility and Support*



*The Business of Science®*

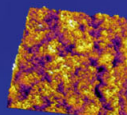


Modulus of Polymers  
& Advanced Materials



Piezoelectrics  
& Ferroelectrics

Coating Uniformity  
& Roughness



Nanoscale Conductivity  
& Permittivity Mapping



+1 (805) 696-6466  
[sales@AsylumResearch.com](mailto:sales@AsylumResearch.com)  
[www.AsylumResearch.com](http://www.AsylumResearch.com)

## Second harmonic generation from metamaterials strongly coupled to intersubband transitions in quantum wells

Salvatore Campione,<sup>1,2,3,a)</sup> Alexander Benz,<sup>1,2</sup> Michael B. Sinclair,<sup>1</sup> Filippo Capolino,<sup>3</sup> and Igal Brener<sup>1,2,b)</sup>

<sup>1</sup>Sandia National Laboratories, Albuquerque, New Mexico 87185, USA

<sup>2</sup>Center for Integrated Nanotechnologies (CINT), Sandia National Laboratories, Albuquerque, New Mexico 87185, USA

<sup>3</sup>Department of Electrical Engineering and Computer Science, University of California Irvine, Irvine, California 92697, USA

(Received 27 January 2014; accepted 20 March 2014; published online 1 April 2014)

We theoretically analyze the second harmonic generation capacity of two-dimensional periodic metamaterials comprising sub-wavelength resonators strongly coupled to intersubband transitions in quantum wells (QWs) at mid-infrared frequencies. The metamaterial is designed to support a fundamental resonance at  $\sim 30$  THz and an orthogonally polarized resonance at the second harmonic frequency ( $\sim 60$  THz), while the asymmetric quantum well structure is designed to provide a large second order susceptibility. Upon continuous wave illumination at the fundamental frequency we observe second harmonic signals in both the forward and backward directions, with the forward efficiency being larger. We calculate the overall second harmonic conversion efficiency of the forward wave to be  $\sim 1.3 \times 10^{-2}$  W/W<sup>2</sup>—a remarkably large value, given the deep sub-wavelength dimensions of the QW structure (about 1/15th of the free space wavelength of  $10 \mu\text{m}$ ). The results shown in this Letter provide a strategy for designing easily fabricated sources across the entire infrared spectrum through proper choice of QW and resonator designs. © 2014 AIP Publishing LLC. [<http://dx.doi.org/10.1063/1.4870072>]

Second harmonic (SH) generation is the process in which an electromagnetic wave at the fundamental frequency (FF) interacting with a nonlinear material leads to the generation of a wave with twice the frequency. SH generation is a powerful phenomenon with wide applicability and has been employed in the development of laser sources,<sup>1–3</sup> optical parametric amplifiers,<sup>4,5</sup> and imaging and microscopy.<sup>6–9</sup>

While the nonlinear optical properties of bulk crystals (e.g., barium borate, lithium niobate, and gallium arsenide) have been extensively investigated in the past,<sup>10–12</sup> more recent work has focused on the nonlinear properties of nano-scale systems such as quantum wells (QWs) and metallic nanostructures. In particular, quantum well systems supporting intersubband transitions (ISTs) have been shown to exhibit extremely large second and third order susceptibilities in the infrared region of the spectrum.<sup>13–16</sup> Furthermore, it has been shown that the SH susceptibilities due to ISTs are generally one to two orders of magnitude larger than that of bulk GaAs, and can be controlled by an external modulating voltage.<sup>17</sup> Recent investigations have also focused on the intrinsic nonlinearity of metamaterials comprising arrays of metal nanostructures,<sup>18–21</sup> along with the use of such metamaterials to enhance the SH generation process from a GaAs substrate.<sup>22,23</sup>

Thus, combining metamaterials with ISTs appears to be a promising strategy for the achievement of large nonlinearities as was recently suggested in Ref. 24. Indeed, metamaterials have recently been used to enable the so-called strong coupling regime between light and ISTs, a regime where the

energy transfer rate between ISTs and a sub-wavelength cavity mode becomes larger than the loss rates present in the system, as detailed in Refs. 25–28 and references therein. In this Letter, we investigate SH generation at mid-infrared frequencies from a strongly coupled system comprising a metamaterial array of sub-wavelength resonators coupled to ISTs in QWs. We show that the giant nonlinear susceptibilities of ISTs along with the metamaterial field enhancements leads to efficient generation of the SH signal. The metamaterial enhances the nonlinear process beyond what can be achieved with other coupling schemes. Due to the sub-wavelength thickness of our QW structure, we are not limited by phase matching conditions<sup>29</sup> as one would have for a conventional nonlinear crystal. Furthermore, our structure does not require a metallic ground plane, so the second harmonic signal can be collected from both forward and backward directions. The investigations performed in this Letter may pave the way for easily fabricated radiation sources in the mid-infrared that do not require population inversion. Moreover, our results can be extended from near- to far-infrared by proper choice of QW material and resonator dimensions.

We first analyze the linear properties of the structure depicted in Fig. 1, where the metamaterial is an array of sub-wavelength gold split ring resonators (SRRs) fabricated on top of a semiconductor heterostructure. The gold permittivity  $\epsilon_{\text{Au}}$  is described using a Drude model<sup>30</sup> with plasma angular frequency of  $2\pi \times 2060 \times 10^{12}$  rad/s and damping rate of  $2\pi \times 10.9 \times 10^{12}$  1/s as done in Ref. 28. The semiconductor heterostructure in Fig. 1 comprises a 30 nm thick Al<sub>0.48</sub>In<sub>0.52</sub>As cap layer with  $\epsilon_c = 10.23$ , and 32 periods of a four layer In<sub>0.53</sub>Ga<sub>0.47</sub>As/Al<sub>0.48</sub>In<sub>0.52</sub>As QW structure, in which the layer thicknesses are 6.1/**1.4**/**3.0**/**10.0** nm (bold numbers

<sup>a)</sup>sncampi@sandia.gov

<sup>b)</sup>ibrener@sandia.gov

represent the  $\text{Al}_{48}\text{In}_{52}\text{As}$  barriers). Importantly, this QW structure supports ISTs at  $\sim 28.1$  THz and  $\sim 57.7$  THz. The overall thickness of the QW region is 656 nm (about  $\lambda_0/15$ , with  $\lambda_0 = 10 \mu\text{m}$  the free space wavelength). The heterostructure is fabricated on an InP substrate with  $\epsilon_s$  given in Ref. 31.

We model the ISTs in QWs as anisotropic Lorentzian dipolar oscillators, leading to a relative dielectric tensor  $\underline{\epsilon}_{\text{IST}} = \epsilon_t(\hat{x}\hat{x} + \hat{y}\hat{y}) + \epsilon_z\hat{z}\hat{z}$ , with  $\epsilon_t = 11.08$  and

$$\epsilon_z = \epsilon_t + \frac{f_{z,12}\omega_{12}^2}{\omega_{12}^2 - \omega^2 - 2i\omega\gamma_{12}} + \frac{f_{z,13}\omega_{13}^2}{\omega_{13}^2 - \omega^2 - 2i\omega\gamma_{13}}, \quad (1)$$

where the first Lorentzian term models the optical transition at 28.1 THz ( $f_{z,12} = 0.67$ ,  $\omega_{12} = 2\pi \times 28.1 \times 10^{12}$  rad/s, and  $\gamma_{12} = 0.04\omega_{12}$ ) and the second term models the transition at 57.7 THz ( $f_{z,13} = 0.16$ ,  $\omega_{13} = 2\pi \times 57.7 \times 10^{12}$  rad/s, and  $\gamma_{13} = 0.04\omega_{13}$ ). [The monochromatic time harmonic convention  $\exp(-i\omega t)$  is implicitly assumed.] The parameters  $\omega_{ij}$  are the IST angular frequencies corresponding to the energies between level  $i$  and level  $j$  of the IST, with level 1 being the ground state,  $2\gamma_{ij}$  represent the IST damping rates, and  $f_{z,ij}$  are proportional to the IST oscillator strengths (computed from the intersubband matrix elements and the carrier concentration as described in Ref. 32). Since the optical transitions only appear in the  $\hat{z}\hat{z}$  component of the permittivity tensor  $\underline{\epsilon}_{\text{IST}}$  only light polarized along the  $z$  direction can interact with the ISTs. While the normally incident radiation has no  $z$ -polarized component, the near-fields of the SRR resonators contain substantial  $z$ -polarized fields that lead to the strong coupling regime. The metamaterial is essential for the generation of  $z$ -polarized fields under normal incidence. A metallic backplane, as is used in Refs. 24 and 33, is however not required for the occurrence of  $z$ -polarized near fields.

The metamaterial structure shown in Fig. 1 is designed to support two resonances: a  $y$ -polarized resonance at  $\sim 30$  THz that we refer to as the FF; and an  $x$ -polarized resonance at  $\sim 60$  THz that we refer to as second harmonic SH. The use of a doubly resonant metamaterial structure supporting resonances at both the FF and the SH has been shown to lead to enhanced SH generation with respect to the singly resonant one.<sup>34,35</sup> For example, in Ref. 34 a 4.6-fold

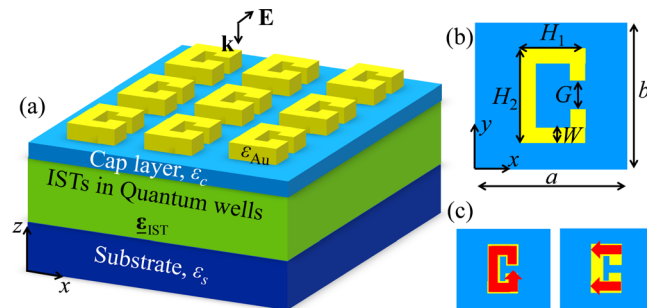


FIG. 1. (a) 3D view of a metamaterial made of SRRs on top of a semiconductor heterostructure. The normal plane wave illumination is explicitly indicated. The SRRs have a thickness of 100 nm here. (b) Top view of the unit cell of the metamaterial in (a). Set of parameters:  $G = W = 0.085$ ,  $H_1 = 0.595$ ,  $H_2 = 0.85$ ,  $a = b = 1.36$  (in  $\mu\text{m}$ ). (c) Sketch of the two main resonant modes of the SRR.

enhancement of the SH efficiency was observed when the metamaterial supported resonances at both the FF and SH.

The simulated normal incidence transmission spectra of our structure without QWs (obtained using FDTD Solutions, commercial finite-difference time-domain software by Lumerical Solutions, Inc.) are shown as black solid lines in Figs. 2(a) and 2(b). The metamaterial exhibits a resonance near 28.2 THz for  $y$ -polarized incident radiation and a second resonance near 61 THz for  $x$ -polarized incident radiation. These frequencies are very close to the IST resonances of 28.1 THz and 57.7 THz as shown in the inset in Fig. 2(b). Upon inclusion of the QWs in the full-wave simulation, we observe a splitting of the resonances around both the FF and the SH [red dashed lines in Figs. 2(a) and 2(b)] due to strong coupling between the metamaterial and the ISTs.<sup>28</sup> Note that the splitting at the FF is larger than the splitting at the SH, which is expected since the IST resonance at 28.1 THz is stronger than the 57.7 THz resonance [inset in Fig. 2(b)]. The two polariton frequencies, i.e., the frequencies corresponding to the two transmission dips, are at 26.7 and 30 THz for  $y$ -polarized incidence, and 56.7 and 63.4 THz for  $x$ -polarized incidence. We refer the reader to Ref. 28 and references therein for more details on the linear properties of strongly coupled structures.

We now consider the nonlinear properties of the structure shown in Fig. 1. The ISTs in QWs are characterized by an anisotropic second order susceptibility tensor with the only non-zero element being  $\chi_{zzz}^{(2)}$ .<sup>15,29</sup> At the FF resonance, the quantum-mechanical expression for  $\chi_{zzz}^{(2)}$  is<sup>13</sup>

$$\chi_{zzz}^{(2)} = -N \frac{e^3}{\hbar^2 \epsilon_0} \frac{z_{12}z_{23}z_{13}}{4\gamma_{13}\gamma_{12}}. \quad (2)$$

In Eq. (2),  $N \cong 6 \times 10^{17} \text{cm}^{-3}$  is the doping concentration (averaged over the entire QW unit cell),  $e = -1.6 \times 10^{-19} \text{C}$  is the electron charge,  $\hbar$  is the reduced Planck constant, and  $z_{ij}$  are the dipole matrix lengths between level  $i$  and level  $j$  of the IST. For this doping level, we have  $z_{12} \cong 1.7 \text{ nm}$ ,  $z_{23} \cong 2 \text{ nm}$ , and  $z_{13} \cong 1.2 \text{ nm}$  (from band structure calculations performed with NextNano3, commercial software by nextnano GmbH). Thus, Eq. (2) leads to  $\chi_{zzz}^{(2)} = 2.5 \times 10^{-7} \text{ m/V}$ , whose order of magnitude is in agreement with previous investigations.<sup>13,15,36</sup> This value for the second order susceptibility is very large when compared to other nonlinear crystals such as barium borate and lithium niobate, whose second order susceptibility is on the order of few to tens of pm/V.<sup>10,11</sup> Such a large value for the susceptibility is required if efficient SH power is to be generated from our extremely thin structure. Note that the SH power cannot be increased by increasing the thickness of the QWs since the strong coupling is based on the near fields of the metamaterial.

Like the linear optical properties, the large second order susceptibility is accessed only through the  $z$ -polarized near fields of the metamaterial resonators, and the SH polarization is thus limited only to the  $z$  direction and is given by  $P_z^{\text{SH}}(2\omega) = \epsilon_0 \chi_{zzz}^{(2)} E_z(\omega) E_z(\omega)$ . Although the on-resonance  $z$ -polarized electric fields do not exhibit a large spatial overlap since the FF field profile is anti-symmetric with respect to the SRR gap, while the SH field profile is symmetric [Figs. 2(c) and 2(d)], the quadratic dependence of the second

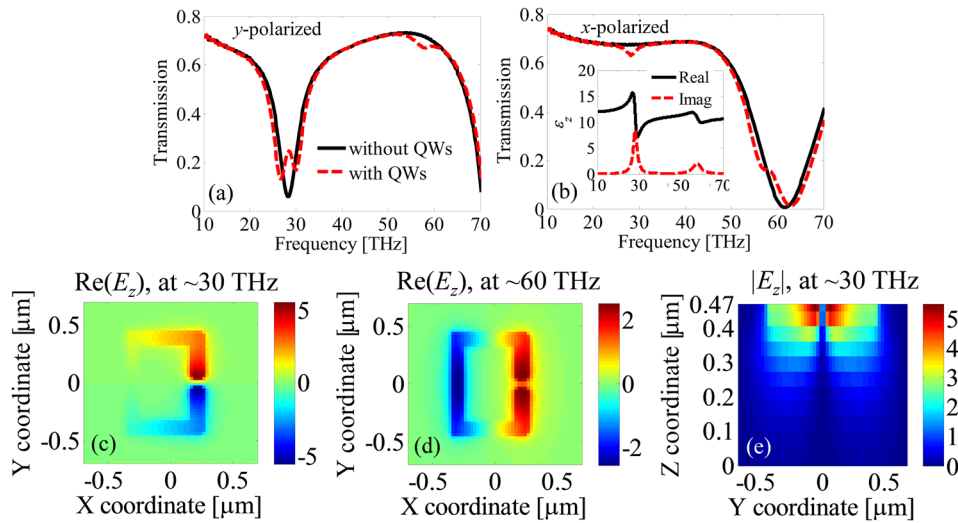


FIG. 2. (a) and (b) Transmission spectra from full-wave simulation for the structure in Fig. 1 under (a) *y*-polarized and (b) *x*-polarized normal plane wave illumination with and without QWs. In (b), the inset shows the real and imaginary parts of the permittivity in Eq. (1). (c) and (d) Real part of the phasor of the *z*-polarized electric field in the *x*-*y* plane at the top of the QW layer excited by (c) *y*-polarized and (d) *x*-polarized waves, at  $\sim 30$  and  $\sim 60$  THz, respectively. (e) Magnitude of the *z*-polarized electric field in the *y*-*z* plane within the QWs at the *x* cut located in the middle of the SRR gap excited by a *y*-polarized wave at  $\sim 30$  THz. We recall that there is no *z*-polarized electric field without the metamaterial.

harmonic polarization on the FF electric field restores the symmetry and allows for good spatial overlap. We stress that without the metamaterial there would be no SH generation under normal incidence because of zero *z*-polarized fields.

We simulate the response of the structure (including the nonlinear susceptibility of the QW region) when illuminated with a normally incident, *y*-polarized, pulsed plane wave. The electric field of the Gaussian pulse is given by

$$\mathbf{E}_i(t) = E_i(t)\hat{\mathbf{y}} = E_0 e^{-\frac{(t-t_0)^2}{2\tau^2}} \sin[\omega(t-t_0)]\hat{\mathbf{y}}, \quad (3)$$

where  $E_0 = 3 \times 10^5$  V/m (corresponding to a peak pump intensity of  $\sim 12$  kW/cm<sup>2</sup>),  $t_0 = 5$  ps is the initial time delay at the plane wave location,  $\tau = 1\text{ps}/(2\sqrt{\ln 2})$  is proportional to the full-width at half maximum (FWHM) of the pulse envelope, and  $\omega = 2\pi f$ , where  $f = 30.25$  THz is the center frequency of the source. We can consider the pump to be a quasi continuous wave because of the large number of optical cycles

$\tau f \cong 20$  within each pulse. The transmitted pulse waveform is then Fourier transformed to obtain its spectral properties.

We show in Fig. 3 the spectra of the *x* and *y* components of the electric and magnetic fields of the transmitted plane wave pulse (similar plots can be obtained also for the reflected pulse). The obtained magnetic fields are related to the electric fields through the wave impedance and consistent with plane wave behavior. The Poynting vector is estimated through  $\mathbf{S} = \pm(\mathbf{E} \times \mathbf{H}^*)/2$ , where an asterisk indicates the complex conjugate operation, and + (−) refers to the backward (forward) direction. It is evident from Fig. 3 that the transmitted pulse is *y*-polarized at the FF and *x*-polarized at the SH. Thus, the FF and SH signals are decoupled in far field and their electric fields are aligned along *y* and *x*, respectively. Also, the FF pump pulse is a transform-limited pulse with a FWHM of  $\sim 1.45\%$  of the center frequency and the SH pulse shows a FWHM of  $\sim 1\%$  of its center frequency.

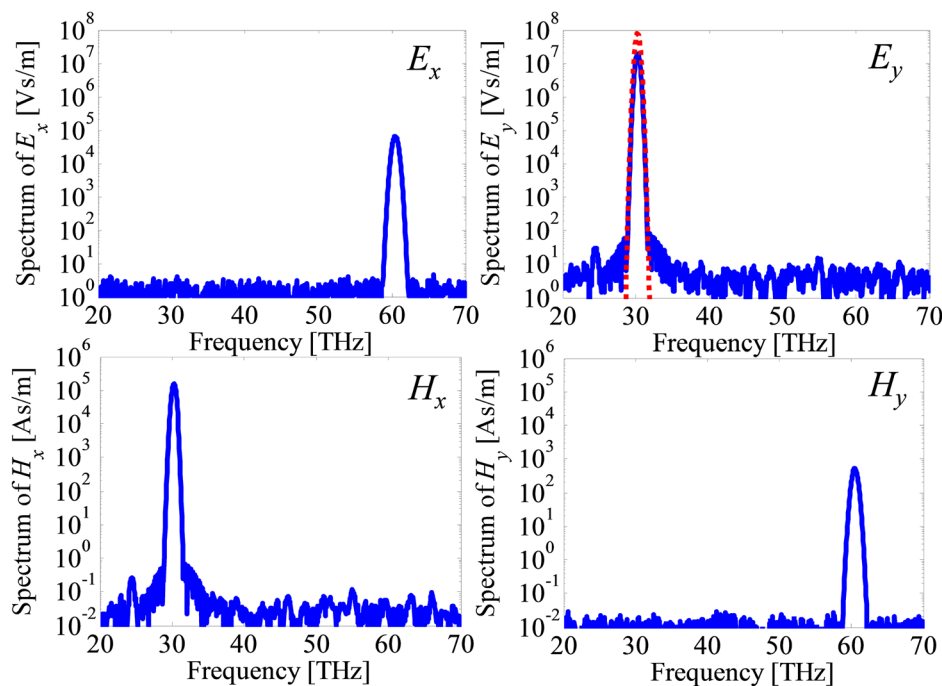


FIG. 3. Spectra of the *x* and *y* components of the electric and magnetic fields of the transmitted pulse for an input pulse centered at 30.25 THz. Peak input intensity is 12 kW/cm<sup>2</sup>. Note the presence of significant SH emitted signal in  $E_x$  and  $H_y$  only. The red dotted line depicts the pump spectrum.

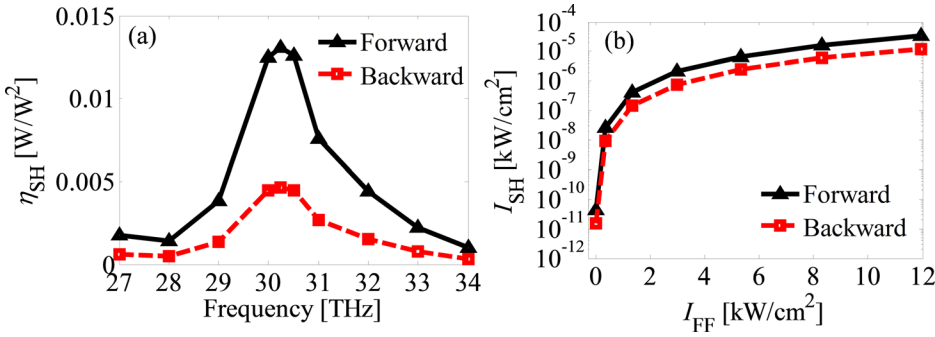


FIG. 4. (a) Conversion efficiency  $\eta_{SH}$  as a function of input pulse center frequency for forward and backward directions for the structure shown in Fig. 1. The peak of the pulsed input intensity is  $12 \text{ kW/cm}^2$ . (b) Intensity at the SH  $I_{SH}$  as a function of pump intensity for forward and backward directions when the input pulse is centered at 30.25 THz.

We then estimate the SH conversion efficiency (in  $\text{W/W}^2$ ) defined as

$$\eta_{SH}^{t,r} = P_{SH}^{t,r}/P_{FF}^2, \quad (4)$$

where  $P_{FF} = I_{FF}A$  is the power at the FF,  $I_{FF}$  is the intensity (the magnitude of the real part of  $S$ ) of the input plane wave at the FF,  $A = ab$  is the metamaterial unit cell area, and  $P_{SH}^{t,r} = I_{SH}^{t,r}A$  is the power at the SH. The superscripts  $t$  and  $r$  indicate the forward (i.e., transmitted) and backward (i.e., reflected) directions.

Under the assumption of an undepleted pump at the FF, we keep the intensity of the  $y$ -polarized input wave fixed at  $12 \text{ kW/cm}^2$  and calculate the efficiency as a function of the input pulse central frequency [see Fig. 4(a)]. We observe that  $\eta_{SH}$  peaks at 30.25 THz and reaches the value of about  $1.3 \times 10^{-2} \text{ W/W}^2$  in the forward direction and of about  $5 \times 10^{-3} \text{ W/W}^2$  in the backward direction. This is a remarkable result given the deep sub-wavelength extent of the QW structure (about  $1/15$ th of the free space wavelength of  $10 \mu\text{m}$ ). If we used a barium borate nonlinear crystal with a refractive index of 1.6 (assuming perfect phase matching),  $\chi^{(2)} = 4 \text{ pm/V}$ , the same thickness as the QW region, and the same excitation conditions, we would obtain  $\eta_{SH} \approx 8.5 \times 10^{-11} \text{ W/W}^2$ , about eight orders of magnitude smaller than the result shown in Fig. 4(a). Furthermore, we report in Fig. 4(b) the intensity at the SH,  $I_{SH}$ , as a function of the intensity at the FF, for both the backward and forward pulses when the input pulse frequency is centered at 30.25 THz. A quadratic dependence of the SH intensity on the input intensity<sup>29</sup> is obtained (i.e.,  $I_{SH}^{t,r} \propto I_{FF}^2$ ). Moreover, the small ratio  $I_{SH}/I_{FF} \approx 3 \times 10^{-6}$  for the largest pump intensity considered in Fig. 4(b) confirms the assumption of undepleted pump.

In conclusion, we have analyzed the SH generation properties of a metamaterial strongly coupled to ISTs in QWs. We find that we can achieve a SH generation conversion efficiency up to  $\sim 1.3 \times 10^{-2} \text{ W/W}^2$  for the forward wave from this deep sub-wavelength QW structure due to the large  $\chi_{zzz}^{(2)}$  and the enhanced electric fields of the resonating metamaterial. Further optimization of the metamaterial geometry and the QW region may lead to larger SH conversion efficiency. Since this structure contains no ground plane we are able to collect second harmonic signal from both forward and backward directions, with a larger  $\eta_{SH}$  in the forward direction. We anticipate that these structures can be used to produce easily fabricated radiation sources at mid-infrared frequencies that do not require population inversion or waveguiding.

This work was performed, in part, at the Center for Integrated Nanotechnologies, a U.S. Department of Energy, Office of Basic Energy Sciences user facility. Portions of this work were supported by the Laboratory Directed Research and Development program at Sandia National Laboratories. Sandia National Laboratories is a multi-program laboratory managed and operated by Sandia Corporation, a wholly owned subsidiary of Lockheed Martin Corporation, for the U.S. Department of Energy's National Nuclear Security Administration under Contract No. DE-AC04-94AL85000.

<sup>1</sup>C. K. N. Patel, *Phys. Rev. Lett.* **15**, 1027–1030 (1965).

<sup>2</sup>U. K. Sapaev, I. A. Kulagin, and T. Usmanov, *J. Opt. B: Quantum Semiclassical Opt.* **5**, 355 (2003).

<sup>3</sup>L. P. Gonzalez, D. C. Upchurch, P. G. Schunemann, L. Mohnkern, and S. Guha, *Opt. Lett.* **38**, 320–322 (2013).

<sup>4</sup>G. Cerullo and S. De Silvestri, *Rev. Sci. Instrum.* **74**, 1–18 (2003).

<sup>5</sup>P. Wasylczyk, I. A. Walmsley, W. Wasilewski, and C. Radzewicz, *Opt. Lett.* **30**, 1704–1706 (2005).

<sup>6</sup>T. Freund and M. Deutsch, *Opt. Lett.* **11**, 94–96 (1986).

<sup>7</sup>R. M. Corn and D. A. Higgins, *Chem. Rev.* **94**, 107–125 (1994).

<sup>8</sup>P. J. Campagnola, A. C. Millard, M. Terasaki, P. E. Hoppe, C. J. Malone, and W. A. Mohler, *Biophys. J.* **82**, 493–508 (2002).

<sup>9</sup>X. Chen, O. Nadiarynkh, S. Plotnikov, and P. J. Campagnola, *Nat. Protoc.* **7**, 654–669 (2012).

<sup>10</sup>W. D. Cheng, J. S. Huang, and J. X. Lu, *Phys. Rev. B* **57**, 1527–1533 (1998).

<sup>11</sup>R. Schiek and T. Pertsch, *Opt. Mater. Express* **2**, 126–139 (2012).

<sup>12</sup>S. Bergfeld and W. Daum, *Phys. Rev. Lett.* **90**, 036801 (2003).

<sup>13</sup>E. Rosencher, P. Bois, J. Nagle, and S. Delaire, *Electron. Lett.* **25**, 1063–1065 (1989).

<sup>14</sup>M. M. Fejer, S. J. B. Yoo, R. L. Byer, A. Harwit, and J. S. Harris, Jr., *Phys. Rev. Lett.* **62**, 1041–1044 (1989).

<sup>15</sup>F. Capasso, C. Sirtori, and A. Y. Cho, *IEEE J. Quantum Electron.* **30**, 1313–1326 (1994).

<sup>16</sup>L. Nevou, M. Tchernycheva, F. Julien, M. Raybaut, A. Godard, E. Rosencher, F. Guillot, and E. Monroy, *Appl. Phys. Lett.* **89**, 151101 (2006).

<sup>17</sup>L. Tsang, D. Ahn, and S. L. Chuang, *Appl. Phys. Lett.* **52**, 697–699 (1988).

<sup>18</sup>M. W. Klein, C. Enkrich, M. Wegener, and S. Linden, *Science* **313**, 502–504 (2006).

<sup>19</sup>M. W. Klein, M. Wegener, N. Feth, and S. Linden, *Opt. Express* **15**, 5238–5247 (2007).

<sup>20</sup>N. Feth, S. Linden, M. W. Klein, M. Decker, F. B. P. Niesler, Y. Zeng, W. Hoyer, J. Liu, S. W. Koch, J. V. Moloney, and M. Wegener, *Opt. Lett.* **33**, 1975–1977 (2008).

<sup>21</sup>N. Pfullmann, C. Waltermann, M. Kovačev, V. Knittel, R. Bratschitsch, D. Akemeier, A. Hütten, A. Leitenstorfer, and U. Morgner, *Appl. Phys. B* **113**, 75–79 (2013).

<sup>22</sup>F. B. P. Niesler, N. Feth, S. Linden, J. Niegemann, J. Gieseler, K. Busch, and M. Wegener, *Opt. Lett.* **34**, 1997–1999 (2009).

<sup>23</sup>W. Fan, S. Zhang, K. J. Malloy, S. R. J. Brueck, N. C. Panoiu, and R. M. Osgood, *Opt. Express* **14**, 9570–9575 (2006).

<sup>24</sup>J. Lee, P. Y. Chen, C. Argyropoulos, A. Alu, and M. A. Belkin, “Metamaterials based on intersubband polaritons,” in *Metamaterials Congress*, Bordeaux, France, 2013.

- <sup>25</sup>J. P. Reithmaier, G. Sek, A. Löffler, C. Hofmann, S. Kuhn, S. Reitzenstein, L. V. Keldysh, V. D. Kulakovskii, T. L. Reinecke, and A. Forchel, *Nature* **432**, 197 (2004).
- <sup>26</sup>G. Gunter, A. A. Anappara, J. H. A. Sell, G. Biasiol, L. Sorba, S. D. Liberato, C. Ciuti, A. Tredicucci, A. Leitenstorfer, and R. Huber, *Nature* **458**, 178 (2009).
- <sup>27</sup>G. Scalari, C. Maissen, D. Hagenmuller, S. De Liberato, C. Ciuti, C. Reichl, W. Wegscheider, D. Schuh, M. Beck, and J. Faist, *J. Appl. Phys.* **113**, 136510 (2013).
- <sup>28</sup>A. Benz, S. Campione, S. Liu, I. Montano, J. F. Klem, A. Allerman, J. R. Wendt, M. B. Sinclair, F. Capolino, and I. Brener, *Nat. Commun.* **4**, 2882 (2013).
- <sup>29</sup>R. Boyd, *Nonlinear optics*, 3rd ed. (Academic Press, New York, 2008).
- <sup>30</sup>M. A. Ordal, L. L. Long, R. J. Bell, S. E. Bell, R. R. Bell, J. R. W. Alexander, and C. A. Ward, *Appl. Opt.* **22**, 1099–1119 (1983).
- <sup>31</sup>E. Palik, *Handbook of Optical Constants of Solids* (Academic Press, New York, 1985).
- <sup>32</sup>A. Gabbay, J. Reno, J. R. Wendt, A. Gin, M. C. Wanke, M. B. Sinclair, E. Shaner, and I. Brener, *Appl. Phys. Lett.* **98**, 203103 (2011).
- <sup>33</sup>A. Benz, S. Campione, S. Liu, I. Waldmueller, J. F. Klem, M. B. Sinclair, F. Capolino, and I. Brener, *Opt. Express* **21**, 32572–32581 (2013).
- <sup>34</sup>T. Kanazawa, Y. Tamayama, T. Nakanishi, and M. Kitano, *Appl. Phys. Lett.* **99**, 024101 (2011).
- <sup>35</sup>M. V. Gorkunov, I. V. Shadrivov, and Y. S. Kivshar, *Appl. Phys. Lett.* **88**, 071912 (2006).
- <sup>36</sup>J. Khurgin, *J. Opt. Soc. Am. B* **6**, 1673–1682 (1989).